

A ground motion model for orientation-independent inelastic spectral displacements from shallow crustal earthquakes

Earthquake Spectra

1–24

© The Author(s) 2023

Article reuse guidelines:

sagepub.com/journals-permissions

DOI: 10.1177/87552930231180228

journals.sagepub.com/home/eqs



Savvinos Aristeidou, M.EERI¹ , Karim Tarbali²,
and Gerard J O'Reilly, M.EERI¹ 

Abstract

The peak inelastic displacement of a single-degree-of-freedom (SDOF) system is an efficient ground motion (GM) intensity measure (IM) for estimating seismic demands in structures and infrastructures. Most ground motion models (GMMs) that predict this IM are developed to estimate the arbitrary or geometric mean of the horizontal GM components obtained from the two as-recorded orientations. In this study, the median and maximum directional inelastic spectral displacements, denoted as $Sd_{i, \text{RotD}50}$ and $Sd_{i, \text{RotD}100}$, respectively, were considered as IMs to develop GMMs. These orientation-independent measures of horizontal motion were calculated by rotating the GMs through all non-redundant rotation angles and have the advantage of removing the sensor orientation as a contributor to overall uncertainty. To do this, several SDOF systems were considered using a subset of the NGA-West2 database to fit GMMs for these IMs. A set of functional forms was developed using a mixed-effects regression approach. The predictor variables were the elastic period, T , the strength ratio, R , and a set of seismological GM causal parameters (i.e. magnitude, distance, soil condition, and so on). Comparison with existing GMMs that consider either inelastic spectral displacement or directionality is provided to highlight key differences and developments. In addition, the response directionality, defined as the ratio $Sd_{i, \text{RotD}100}/Sd_{i, \text{RotD}50}$, was observed to be notably impacted by the strength ratio and elastic period, which has not been discussed in the literature to date. Overall, this GMM has the advantage of quantifying ground motion intensity via an efficient IM in Sd_i , which can better highlight some fundamental issues surrounding the directionality of GMs and allow for more informative risk estimates.

¹Centre for Training and Research on Reduction of Seismic Risk (ROSE Centre), Scuola Universitaria Superiore IUSS Pavia, Pavia, Italy

²CentraleSupélec, Université Paris-Saclay, Gif-sur-Yvette, France

Corresponding author:

Gerard J O'Reilly, Scuola Universitaria Superiore IUSS Pavia, Palazzo del Broletto, Piazza della Vittoria 15, Pavia 27100, Italia.

Email: gerard.oreilly@iusspavia.it

Keywords

Ground motion model, directionality, inelastic spectra, *RotD50*, *RotD100*, intensity measure

Date received: 21 December 2022; accepted: 18 May 2023

Introduction

An accurate representation of the expected damage is needed in any urbanized area for disaster risk management and urban planning. This requires utilizing appropriate ground motion (GM) intensity measures (IMs) that characterize the response of nonlinear structural systems. Seismic hazard and structural response analyses often use single or multiple IMs (Baker and Cornell, 2005; Bradley, 2012; O'Reilly, 2021; Vamvatsikos and Cornell, 2005) to represent shaking intensity. Empirical ground motion models (GMMs) provide the probabilistic distributions of these IMs and allow representative GMs to be selected for nonlinear response history analyses (NRHAs) and estimate structural demands. The most common scalar IM currently used is the spectral acceleration Sa at a given period T of vibration, $Sa(T)$. The notation Sa will be used for brevity herein, implying the spectral acceleration at a period T and 5% of critical damping. Since seismic shaking is felt principally as shaking in three dimensions, there is a need to consider the possible effects of GM directionality, which is illustrated graphically in Figure 1. Here, “Displacement X” denotes the displacement of the oscillator in the first as-recorded direction as given from the database, and similarly “Y” in the second as-recorded direction. As shown, different GMs may induce significantly different directional demands on a system, and a given GM may induce different directional demands on different systems. Notably, Baker and Cornell (2006) addressed this question by discussing the regular use of an arbitrary Sa component, Sa_{arb} , or the geometric mean of the two as-recorded Sa components, Sa_{gm} , in seismic analyses.

In recent years, various Sa definitions have been proposed that may be considered more representative of the ground shaking in the entire two-dimensional (2D) horizontal plane.

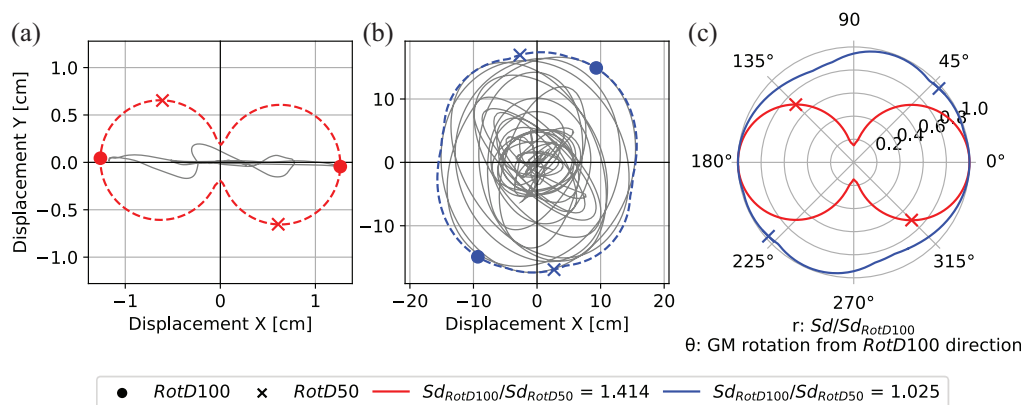


Figure 1. Trace response of an elastic SDOF oscillator with $T = 2$ s.

(a) Strongly polarized GM, SMART1 O07 recording from the 1985 Taiwan SMART1(33) earthquake, RSN: 492; (b) unpolarized GM, Dumbarton Bridge West End FF recording from the 1989 Loma Prieta earthquake, RSN757; and (c) polar plot of normalized spectral displacement in all horizontal directions for the two considered records in this figure (color version available online).

Some of these definitions include the different percentiles of Sa over all non-redundant orientations of elastically responding systems (Boore, 2010; Boore et al., 2006; Rupakhety and Sigbjörnsson, 2013). Boore (2010) defines the $RotD_{nm}$ component of Sa as the m^{th} percentile of all rotation angles sorted by amplitude, with D denoting the period-dependent rotation angle. The vast majority of modern GMMs of the NGA-West2 project adopt *ad nauseam* the $RotD50$ horizontal component definition (Bozorgnia et al., 2014). Therefore, it was considered thematic to extend and propose herein inelastic response values as an IM with the same horizontal component definition but with additional flexibility, which to the authors' knowledge, does not exist in the literature. These Sa definitions (e.g. $RotD100$, $RotD50$, and $RotD00$) have been shown to more accurately represent the directional dependency of GMs in the horizontal plane (Baker and Lee, 2018; Bradley, 2010; Tarbali, 2017). They have been used in several studies to quantify the directional response of both elastic (Bradley and Baker, 2014) and inelastic single-degree-of-freedom (SDOF) systems (Ahdj et al., 2020; Burks and Baker, 2014; Zengin and Abrahamson, 2021). In addition, the NGA-West2 database (Ancheta et al., 2013) was used (Shahi and Baker, 2014) to develop an empirical model for the ratio between $Sa_{RotD100}/Sa_{RotD50}$ and quantify the directionality measure (i.e. polarization) of horizontal GM pairs, as illustrated in Figure 1. This was mainly carried out to enable the estimation of $Sa_{RotD100}$ response spectra from Sa_{RotD50} spectral ordinates via an empirical model proposed by those authors.

On one hand, many insights have been obtained from these studies concerning the impacts of directionality on linear systems. On the other hand, studies on complex non-linear systems have drawn many interesting structure-specific conclusions. Several researchers have also developed GMMs for peak inelastic spectral displacements of SDOF systems, Sd_i , (Heresi et al., 2018; Huang et al., 2020; Rupakhety and Sigbjörnsson, 2009; Stafford et al., 2016; Tothong and Cornell, 2006). Under certain conditions, Sd_i has been demonstrated to be an effective IM to relate GM intensity and inelastic structural response and, therefore, the structural and non-structural damage of engineered systems (Aslani and Miranda, 2005; Luco and Cornell, 2007).

In this study, the $RotD_{nm}$ for the 00th, 50th, and 100th percentiles of Sd_i are investigated for all non-redundant incidence angles for bilinear SDOF systems with a range of T and strength ratios, R . The latter parameter is defined as the ratio of the elastic strength demand to the inelastic strength demand (i.e. the reduction due to nonlinear hysteretic behavior; Miranda and Bertero, 1994), and is discussed in more detail later. From the resulting data, an empirical GMM is developed, with the predictor variables being T , R , and a set of seismological parameters. These are common predictor variables used in many other GMMs, but herein there is the addition of R , which can be challenging to estimate with high degree of accuracy for a building portfolio. In such a case, it is assumed that even approximate values of T and R can still make for an efficient IM for regional risk assessment, which can possibly outperform classic IMs—for example, peak ground acceleration (PGA) or $Sa(T_1)$ that do not take into account the nonlinear behavior of the structure—with a little extra effort. In the case of a single building assessment, knowing the yield/capping horizontal force, the R can in principle be obtained for a given return period or shaking scenario. Hence, it is hypothesized that this trade-off between the estimation of one more parameter and the additional benefits gained by using it is worth considering.

The goal of this GMM is not only to predict a useful IM well-correlated with structural demand but also to give an expected measure of directionality for certain conditions. Hence, it can provide important insights into the maximum directional response of

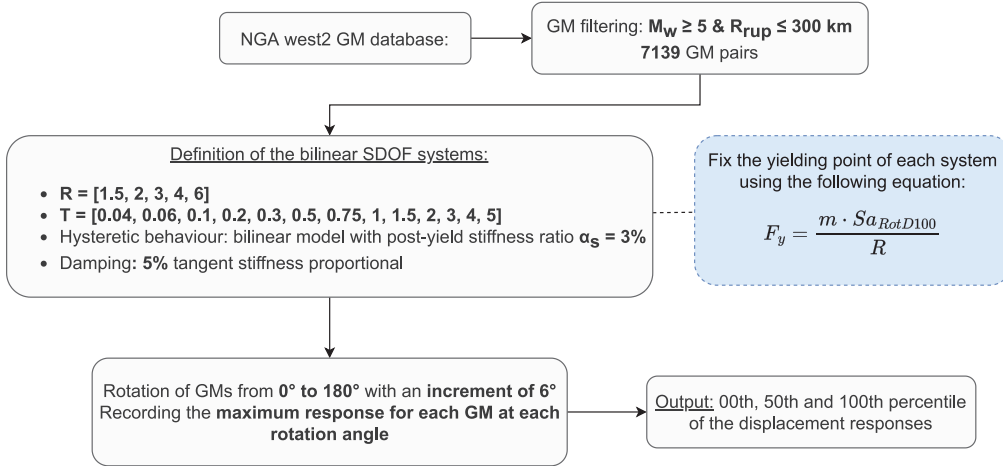


Figure 2. Illustration of the methodology adopted to generate data (color version available online).

inelastic systems, enabling a more comprehensive quantification of seismic damage to engineered structures. The GMM was also fitted for the *RotD100* horizontal component definition, as it can be used in important structures where the maximum response in the horizontal plane is of interest. Modern seismic design codes have also included the use of *RotD100* horizontal component in their provisions, namely (American Society of Civil Engineers (ASCE)/SEI 7-16, 2018) in their “risk-targeted maximum considered earthquake (MCE_R) ground motion hazard analysis.” To give more insight on the importance of these IMs, if the case of a linear isotropic structure is considered and its resultant displacement is the desired output, then the $Sa_{RotD100}$ would be the best predictor. However, when the system is nonlinear and isotropic, the $Sd_{i,RotD100}$ of the equivalent SDOF system would be a much more representative predictor of the resultant displacement. In addition, when a regular structure is modeled in its two principal directions, the GMs can be selected and scaled to represent the median or maximum directional inelastic response, utilizing the two *RotD50* and *RotD100* definitions proposed in this study. In any case, it should be noted here that there is a distinction between the *RotDnn* component of the inelastic SDOF system (i.e. horizontal component definition of the IM), and the *RotDnn* of the actual structure’s response.

In the following sections, an overview of the workflow followed is outlined, describing the GM database and GMM functional forms used along with the analyses that went into the development of the model. This is then appraised via a performance comparison of the model and the relative differences with different, but similar, models available in the literature.

Methodology

The methodology employed to generate the data for the model calibration is outlined in Figure 2. First, the GMs within the range of M_w and R_{rup} of interest were extracted from the NGA-West2 database and are discussed in the next section. Then, the range of R and T values, along with the hysteretic behavior, post-yield stiffness, and the damping of the SDOF system, were defined. For each SDOF system, the GMs were rotated with an

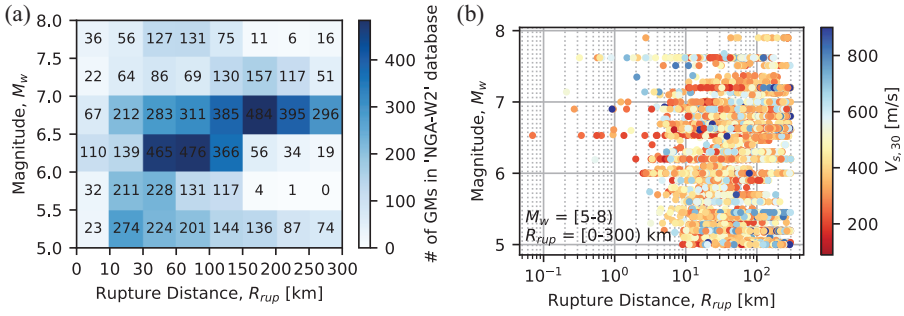


Figure 3. Distribution of the considered GMs used in terms of (a) M_w - R_{rup} bins and (b) scatter plot depicting the $V_{s,30}$ (color version available online).

increment of 6° in the range of 0° to 180° and applied to the numerical model developed in OpenSeesPy (Zhu et al., 2018) to obtain the peak displacement. The elastic $Sa_{RotD100}$ and Sa_{RotD50} of each GM were acquired from the meta-data in the flatfile of the NGA-West2 database. The total number of analyses presented in this study amounted to $7139 \text{ GMs} \times 5 \text{ R} \times 13 \text{ T} \times 30$ incidence angles to give 13,921,050 inelastic SDOF analyses. These computational analyses are needed because for inelastic response values, the $RotD_{mm}$ component cannot be interpreted in terms of the principal components of the as-recorded motion since the linear relationship and transformability breaks down once the system becomes inelastic.

Strong motion database

The GM records used in this study were obtained from the NGA-West2 database (Ancheta et al., 2013), which is a comprehensive database of shallow crustal earthquakes in active tectonic regions. From this database, a subset of GMs recorded during earthquakes deemed of sufficient intensity to cause structural and/or non-structural damage was selected for the analyses. Specifically, the subset considered was earthquakes whose $M_w \geq 5$ and $R_{rup} \leq 300$ km. The considered earthquakes distributed in different M_w - R_{rup} bins are shown in Figure 3a. This subset includes 7139 recordings from 200 earthquake events, whose scatter plot of M_w , R_{rup} , and $V_{s,30}$ is depicted in Figure 3b. Note that the maximum $V_{s,30}$ value in the selected GM pool reached 1289 m/s, but everything above 900 m/s is plotted with the same dark blue color for clarity. It can be seen that most of the earthquakes had M_w between 6 and 7 and R_{rup} between 30 and 250 km. In addition, GMs with the maximum usable periods lower than the elastic period of the corresponding system in each case were filtered out of the considered GM subset for a given SDOF system.

Description of SDOF systems

The SDOF system chosen for this study was a bilinear model with positive strain hardening ratio $\alpha_s = 3\%$, shown in Figure 4. The hysteretic behavior of this system is non-degrading and non-evolutionary. A tangent stiffness proportional damping model was adopted with a ratio of $\xi = 5\%$. The range of elastic periods considered was $T = 0.04, 0.06, 0.1, 0.2, 0.3, 0.5, 0.75, 1, 1.5, 2, 3, 4, 5$ in seconds, and the set of strength ratios was $R = 1.5, 2, 3, 4, 6$ (Figure 2). The strength ratio, also known as force reduction factor, R , is defined as the ratio of maximum spectral demand in the elastic system with period T

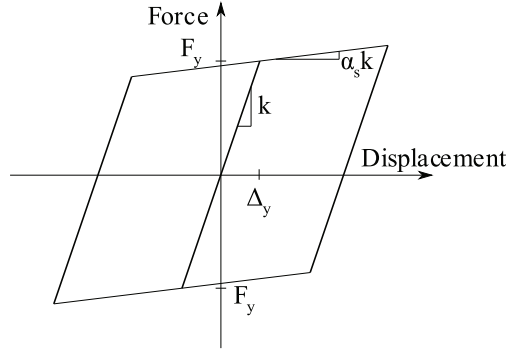


Figure 4. Hysteretic behavior of the bilinear SDOF model.

subjected to a given GM, F_{el} , to the SDOF yield strength, F_y . In practice, this meant that for a given period T and R pair, along with a GM whose $Sa_{RotD100}$ is known, F_y is computed by Equation 1, where m is a nominal value of mass, meaning that any value can be chosen since it will then be modeled in the numerical model also.

$$F_y = \frac{m S a_{RotD100}}{R} \quad (1)$$

The aim of using this kind of standardized SDOF system is to represent the inelastic displacement demand of a wide range of first-mode-dominated multi-degree-of-freedom (MDOF) systems and not any specific typology. This gives the opportunity to study the general trends on inelastic response spectra. Future work may consider the response of hysteretic models that represent different structural systems.

Investigating directional inelastic displacement spectra trends

Following the workflow outlined in Figure 2, the data for all SDOF system combinations were generated. To examine these, this section first investigates the trends observed for the directional inelastic displacement spectra to be used in the functional form fitting. In addition, the degree of directionality is discussed along with the observed ductility demands and the impacts of near and far fault GMs.

Computation of $Sd_{i,RotDnn}$ spectra

The 84th, 50th, and 16th percentiles of the elastic, $Sd_{e,RotDnn}$, and inelastic, $Sd_{i,RotDnn}$, spectral displacements are shown in Figure 5. These were generated using the numerous response points obtained from the SDOF analyses but binning the data and computing the relevant percentiles. The $RotD00$ (i.e. the minimum directional response) of the inelastic response is also considered in the comparisons. Generally, it can be seen from Figure 5a and b that for $T < 1$ s, the median Sd_i increases with R , while for $T > 1$ s, the inelastic response is close to the elastic response. This was an expected result, as the nonlinear behavior of medium to long-period structures typically follows the equal-displacement approximation (Chopra, 2014), where for shorter periods the nonlinear response tends to be higher, as observed. This was also presented in the study by Huang et al. (2020) and holds true for different inelastic $RotDnn$ quantities, hence being reconfirmed here.

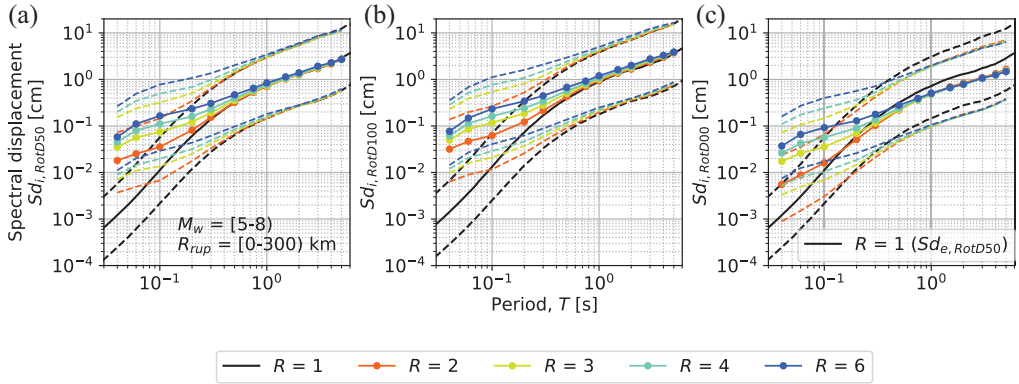


Figure 5. Inelastic spectral displacement defined via the median (solid lines) and 16th and 84th percentiles (dashed lines) for the (a) *RotD50*, (b) *RotD100*, and (c) *RotD00* components of response (color version available online).

Figure 5c compares the *RotD50* elastic displacement spectrum (shown in black) with the *RotD00* of the inelastic displacement spectrum. This investigated whether the elastic *RotD50* response, conventionally used in the seismic design process, can be higher than the minimum inelastic response. It is interesting to see that the inelastic *RotD00* can, in fact, be higher than the elastic *RotD50* for $T \leq 0.3$ s. For longer periods, the aforementioned inelastic response is always lower than the elastic one, which is the general result that was expected. This shows that the elastic response cannot sufficiently represent the minimum directional response of inelastic systems with short T .

Impact of inelastic behavior on directionality response

The next aspect of the SDOF system response was the degree to which the nonlinear behavior can impact the directionality of the response. To do this, a way in which the GM directionality could be quantified was needed. From the literature, the *RotD100*/*RotD50* ratio of Sd_i was identified as a suitable choice as it describes how much the response tends to be polarized and has been illustrated in Figure 1. Computing this ratio for all of the cases previously described in Figure 5a and b was done and the results are summarized in Figure 6.

As a first comparison, Figure 6a shows the geometric mean of *RotD100*/*RotD50* ratio for the elastic (i.e. $R = 1$) systems and compares them with the corresponding values previously published by Shahi and Baker (2014), denoted as SB14. It can be seen that the directionality measure for the selected range of GMs is in good agreement with this model previously developed. This is also the case for the standard deviations shown in Figure 6b. In the case of elastic SDOF systems, the *RotD100*/*RotD50* ratio can range from 1 for unpolarized GMs to $\sqrt{2}$ for extremely polarized ones from basic geometric definitions. However, this directionality measure can reach much higher values for inelastic systems, with the lower bound staying the same. Figure 6a shows that for $T > 0.3$ s, the geometric mean of *RotD100*/*RotD50* ratio tends to increase as R increases, meaning the more nonlinearity expected in the structural system, the more its response can be anticipated to become polarized. However, it is important to note that the *RotD100*/*RotD50* ratios approach the elastic one for $T > 0.5$ s, especially for low R values.

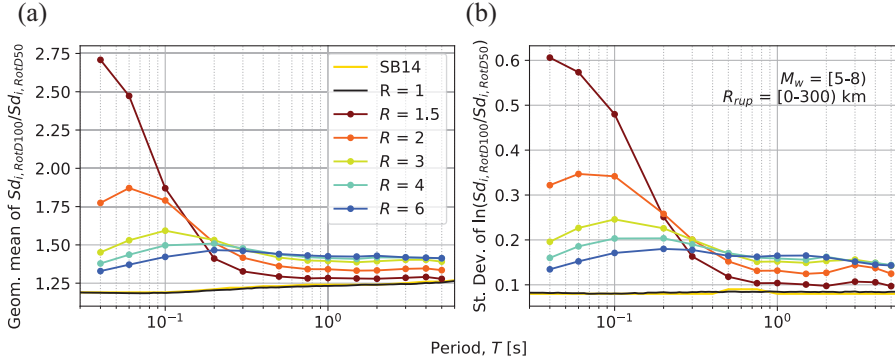


Figure 6. Impact of inelastic behavior on directionality response shown via the (a) geometric mean and (b) logarithmic standard deviation of the $Sd_{i, RotD100}/Sd_{i, RotD50}$ ratio for different values of T and R . SB14 is the Shahi and Baker (2014) model for the elastic $RotD100/RotD50$ ratio (color version available online).

However, for $T < 0.3$ s, the SDOF systems with lower R factors exhibit a more pronounced impact of directionality, reaching the value of 2.7. This is a notable observation as it essentially means that the trend for medium to long periods tends to reverse for shorter periods, but still returns back to the elastic ratio previously computed by Shahi and Baker (2014). Several R factors were considered, and it was seen that for $R = 1.5$ – 2.5 these impacts were most notable. Similar conclusions were drawn by Fontara et al. (2015), where for a structural system of $T = 0.3$ s the variability of structural response to the seismic incidence angle became larger as the level of structural nonlinearity increased. The dispersion of the directionality measure, calculated as the standard deviation of the natural logarithm of the directionality measure, is presented in Figure 6b. It can be seen that the overall trend is similar to the corresponding geometric mean curves. The logarithmic standard deviation is minimized and approaches the elastic system for long T . Similar to what was done in the study by Shahi and Baker (2014), a mixed-effects regression was fitted to the data to develop directionality models for inelastic spectral displacements. A table is provided as an electronic supplement containing the inter-, intra-event, and total logarithmic standard deviation, along with the mean of $\ln(Sd_{i, RotD100}/Sd_{i, RotD50})$, named “inel_dirac_model.xlsx.” These can be used to transform the inelastic spectra obtained from other GMMs from the RotD50 to RotD100 definition.

Impact of directionality on expected displacement ductility ratio

While the comparisons shown so far have focused on the observations regarding $Sd_{i, RotD100}$ and $Sd_{i, RotD50}$ spectra, it is also interesting to note how these inelastic displacements compare to the nonlinear spectra typically used in seismic design and assessment. These are the so-called R - μ - T relationships and can be found in several past studies (Miranda and Bertero, 1994; Nafeh et al., 2020; Newmark and Hall, 1982; Vamvatsikos and Cornell, 2006; Vidic et al., 1994) and implemented in numerous methods and codes of practice. These past models typically adopt an arbitrary component of the GM, $Sd_{i, arb}$, in their definition, so it is interesting to see how much of an impact changing to $Sd_{i, RotD100}$ would have. Figure 7a depicts the median displacement ductility calculated as $\mu_{RotD100} = Sd_{i, RotD100}/\Delta_y$ versus T for the considered R factors. It can be seen that, for a given R factor, μ decreases as T increases until it generally plateaus for $T > 1$ s. This is

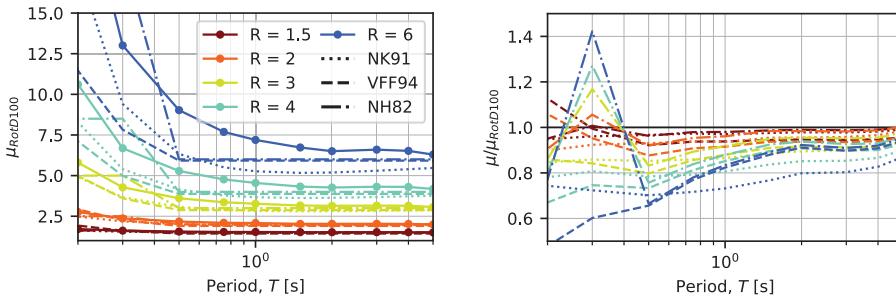


Figure 7. Comparison of the relationship between strength ratio, R , period of vibration, T , and the ductility demand observed in the SDOF systems when considering the $Sd_{i,RotD100}$ or the $Sd_{i,arb}$ used in conventional models (color version available online).

essentially due to the nonlinear behavior of the systems converging toward the equal-displacement approximation, meaning that $R \approx \mu$.

Three well-established models relating R , μ , and T from the literature by Nassar and Krawinkler (1991), Vidic et al. (1994) and Newmark and Hall (1982), denoted NK91, VFF94, and NH82, respectively, are also plotted in Figure 7 for comparison. It can be seen that the trend of those models is very close to the trend of the results obtained here. Nonetheless, the median values estimated in this study are somewhat higher, especially for the systems with high R factors and short T . This can be observed in Figure 7b via the $\mu/\mu_{RotD100}$ ratio where for moderate inelasticity and $T < 1$ s, the maximum response can be underestimated by NK91, VFF94, and NH82 by up to 40%, whereas this reduced to 10%–20% for longer periods.

These differences are primarily due to two reasons. First, while the other studies were performed for the arbitrary as-recorded components of GMs, the ductility presented here is for the system's 100th percentile response direction. Second, although both previous studies used bilinear hysteretic models, there are slight differences in the post-yield stiffness and the assumption of viscous damping modeling. Furthermore, Nassar and Krawinkler (1991) considered 15 GMs in the western United States and Vidic et al. (1994) considered 20 GMs recorded in the western United States and the 1979 Montenegro earthquake, as opposed to the 7167 GMs considered in this study.

Near- and far-fault GMs

To examine the distinction in nonlinear response observed from near-fault and far-fault GMs, different bins were examined in terms of the directional inelastic response (i.e. $Sd_{i,RotD100}$ and $Sd_{i,RotD50}$) and the directionality measure (i.e. $Sd_{i,RotD100}/Sd_{i,RotD50}$) depicted in Figure 8. A comparison of the inelastic spectra shows that near-fault GMs result in higher elastic and inelastic displacements across the entire range of periods. It is also apparent from Figure 8c that the near-fault GMs result in higher directionality in the nonlinear systems. This is especially true for moderate ductility (lower R factor) structures. A similar trend is also present for the elastic systems. These observations are to be expected as it is well-known that near-fault GMs exhibit higher directional effects (Bray and Rodriguez-Marek, 2004; Huang et al., 2009; Tarbali, 2017; Tarbali et al., 2019).

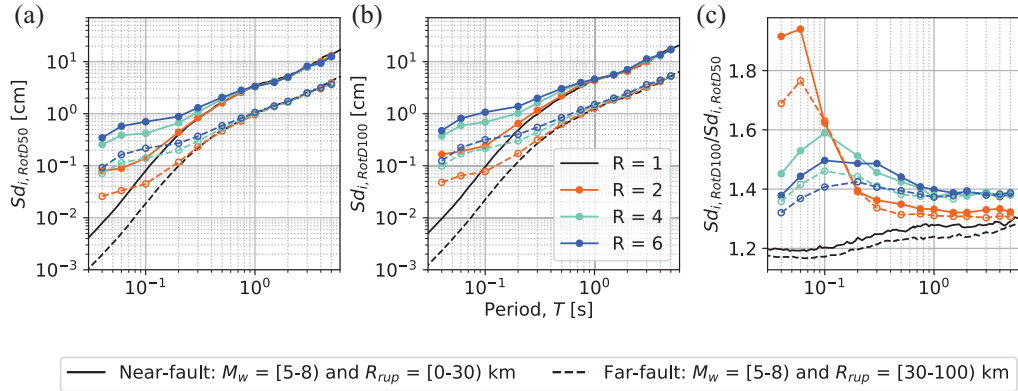


Figure 8. Comparing the impact of near- and far-fault ground motions via the (a) median $Sd_{i, RotD100}$ spectra, (b) median $Sd_{i, RotD50}$ spectra, and (c) median directionality measure ($Sd_{i, RotD100}/Sd_{i, RotD50}$; color version available online).

Fitting of a GMM

Functional form

Utilizing the results presented previously, this section presents a simple, but accurate, model to predict the $RotD50$ and $RotD100$ of the peak inelastic displacement demands of the considered SDOF system for a given T and R using a set of explanatory parameters. The main functional form of this model, which was chosen after many trial combinations of functional forms from past GMMs examining inelastic spectral displacement (Bozorgnia et al., 2010; Heresi et al., 2018; Huang et al., 2020), is given by:

$$\ln Y_{i,j} = a + F_M + F_D + F_{sof} + F_s + F_{basin} + \eta_i + \varepsilon_{i,j} \quad (2)$$

where, $Y_{i,j}$ is the m^{th} orientation-independent component of peak inelastic spectral displacement demand $Sd_{i, RotDmn}$ (in centimeters) at site j in event i ; a is a constant coefficient; F_M , F_D , F_{sof} , F_s , F_{basin} are the magnitude scaling, distance function, style of faulting, site amplification, and the basin-effects correction terms, respectively. While the m may refer to any percentile of the $RotDmn$ component, this GMM was limited to predicting only the 50th and 100th. The model given in Equation 2 separates the inter- and intra-event residuals (i.e. mixed-effects model). It also considers the inherent correlation of all the samples from the same event, in contrast to a model with a single residual term (i.e. fixed model) that assumes all samples to be independent. η_i is the event term corresponding to event i following a normal distribution with zero mean and standard deviation τ ; $\varepsilon_{i,j}$ is the intra-event error term corresponding to event i at station j following a normal distribution with zero mean and standard deviation φ . It should be noted that η_i and $\varepsilon_{i,j}$ are assumed to be mutually independent; therefore, the total standard deviation of the model is calculated as:

$$\sigma = \sqrt{\tau^2 + \varphi^2} \quad (3)$$

The magnitude function in Equation 2, which does not consider magnitude saturation is given by:

$$F_M = b_1(M_{w,i} - M_r) + b_2(M_{w,i} - M_r)^2 \quad (4)$$

where, M_w is the moment magnitude, M_r is the reference magnitude taken here to be equal to 6, and b_1 and b_2 are unknown model fitting coefficients. The distance function is:

$$F_D = [c_{1k} + c_{2k}(M_{w,i} - M_r)] \ln\left(\frac{R_{mod}}{R_{h2}}\right) \begin{cases} k = 1; & R_{mod} \leq R_{h1} \\ k = 2; & R_{h1} < R_{mod} \leq R_{h2} \\ k = 3; & R_{mod} > R_{h2} \end{cases} \quad (5)$$

where R_{mod} is a modified distance to the source computed given as:

$$R_{mod} = \sqrt{R_{rup}^2 + c_3^2} \quad (6)$$

where R_{rup} is the closest distance from the rupture plane to the site in kilometers, c_3 is a model coefficient, and c_{1k} and c_{2k} are attenuation coefficients. R_{h1} and R_{h2} are hinge distances to account for the changes in the attenuation rate and are fixed to 15 and 150 km, respectively, and the index k is introduced to account for the different distance ranges. The style-of-faulting function is given as:

$$F_{sof} = f_1 F_{N,i} + f_2 F_{T,i} \quad (7)$$

$$(F_{N,i}, F_{T,i}) = \begin{cases} (0, 0); & \text{Strike - slip fault} \\ (1, 0); & \text{Normal fault} \\ (0, 1); & \text{Thrust fault} \end{cases}$$

where, f_1 and f_2 are model fitting parameters; F_N and F_T are dummy variables representing the style of faulting. The site amplification function is given by:

$$F_s = s_n \cdot \ln(V_{s,30}) \begin{cases} n = 1; & V_{s,30} < 400 \\ n = 2; & 400 \leq V_{s,30} < 650 \\ n = 3; & 650 \leq V_{s,30} < 1000 \\ n = 4; & V_{s,30} \geq 1000 \end{cases} \quad (8)$$

where, s_n is a model fitting coefficient parameter with the index n differentiating between the different $V_{s,30}$ bins, where $V_{s,30}$ is in meters per second. The basin-effects correction is given as:

$$F_{basin} = \begin{cases} d_1(Z_{2.5} - 1); & Z_{2.5} \leq 1 \\ 0; & 1 < Z_{2.5} \leq 3 \\ d_2[1 - e^{-0.25(Z_{2.5}-3)}]; & Z_{2.5} > 3 \end{cases} \quad (9)$$

where, d_1 and d_2 are model fitting coefficients, and $Z_{2.5}$ is the depth to the 2.5 km/s shear-wave velocity horizon, typically referred to as basin or sediment depth in kilometers. For the records without registered $Z_{2.5}$, the guidelines suggested in the study by Kaklamanos et al. (2011) were followed, utilizing the formulae given in the studies by Abrahamson and Silva (2008) and Campbell and Bozorgnia (2007) to estimate $Z_{2.5}$ from $V_{s,30}$. Specifically, if $Z_{1.5}$ is known, then the following equation may be used, where all depths are in meters:

$$Z_{2.5} = 636 + 1.549Z_{1.5} \quad (10)$$

If $Z_{1,0}$ is known (but $Z_{1,5}$ is unknown), then $Z_{2,5}$ may be estimated by the following extrapolation:

$$Z_{2,5} = 519 + 3.595Z_{1,0} \quad (11)$$

When $Z_{1,0}$ is also unknown, the following equation may be used to estimate $Z_{1,0}$ from $V_{s,30}$:

$$Z_{1,0} = \begin{cases} \exp(6.745) & \text{for } V_{s,30} < 180 \text{ m/s} \\ \exp\left[6.745 - 1.35 \cdot \ln\left(\frac{V_{s,30}}{180}\right)\right] & \text{for } 180 \leq V_{s,30} < 500 \text{ m/s} \\ \exp\left[5.394 - 4.48 \cdot \ln\left(\frac{V_{s,30}}{500}\right)\right] & \text{for } V_{s,30} > 500 \text{ m/s} \end{cases} \quad (12)$$

For each SDOF system and combination of R and T , the model parameters required to fit the expressions represented by Equation 2 were computed. The standard deviations τ and φ were computed through a series of iterative random-effects nonlinear regressions, following the one-stage mixed-effects regression algorithm proposed by Abrahamson and Youngs (1992). The “trust region reflective” method was used for the fixed-effects regression with least squares, which is the first step of this algorithm. This is particularly suitable for large sparse problems with bounds and is generally a robust method. Different methods were tested for the nonlinear least-squares regression, showing a good similarity between each. Following this approach, the resulting empirical coefficients and standard deviations are made available in an electronic supplement.

GMM performance

To assess the performance of the model against the observed data, a visual inspection of the residuals was carried out. A residual is defined as the difference between the “observed empirical data” (i.e. the computed peak inelastic displacements according to the methodology described in Figure 2) and the model prediction, both in natural logarithm. Herein, a positive residual indicates underprediction by the proposed model.

Figure 9 depicts the inter-event residuals versus the event magnitude for both the $Sd_{i,R0tD50}$ and $Sd_{i,R0tD100}$ component of response and four different combinations of T and R . Plotted in the same figure are also the binned mean residual values, ± 1 standard deviation. These results clearly indicate that the functional form chosen adequately represents the event term, as no apparent bias against M_w is observed. This trend was also observed across the entire range of T and R used in this study.

Figure 10 then shows the total residuals of the same cases with respect to R_{rup} for four different combinations of T and R . Again, the binned means ± 1 standard deviation are plotted to show that they do not consistently deviate from zero as a function of distance. This lack of trend indicates that the functional form adopted is adequate for capturing the data trends.

Figure 11 shows the total residuals as a function of $V_{s,30}$ for different combinations of T and R for both $Sd_{i,R0tD50}$ and $Sd_{i,R0tD100}$. As per Equation 8, this site amplification term was separated into four bins in between $V_{s,30} = 400, 650$ and 1000 m/s, which were established based on visually inspecting the total residuals versus $V_{s,30}$ and their deviation from zero in certain ranges. This was necessary to capture the main trends in the response

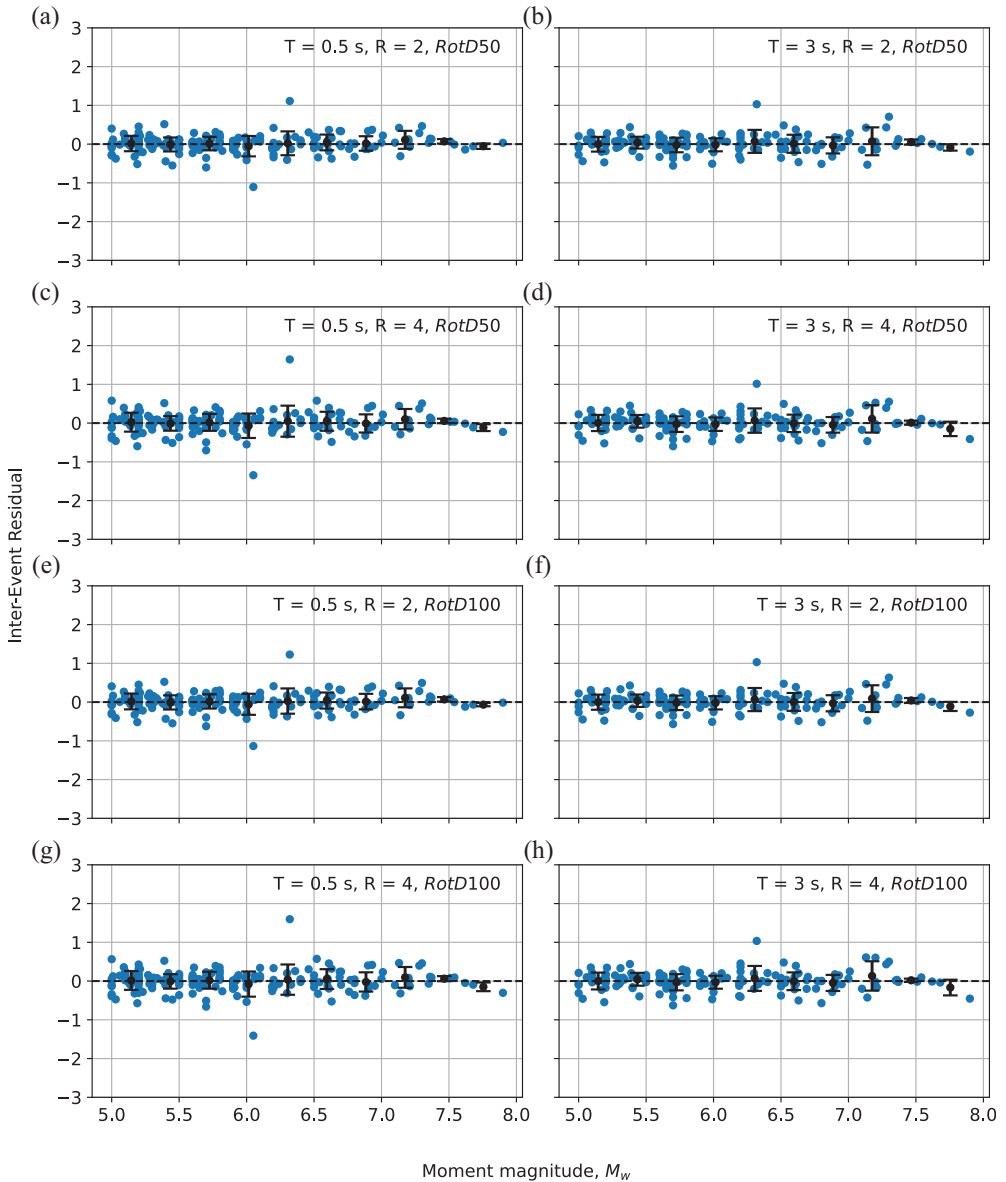


Figure 9. Inter-event residuals with respect to M_w for different T and R . Blue dots represent the observed residuals, while black dots and error bars represent the binned mean and \pm one standard deviation, respectively (color version available online).

amplification due to the soil conditions, where it can be seen from Figure 11 that the model does not exhibit any significant bias with respect to the $V_{s,30}$ of the site.

For a visual inspection of the three aforementioned figures, it can be seen that the model fits well for both the *RotD50* and the *RotD100* components, with the *RotD100* component presenting slightly higher standard deviations.

Overall, the previous figures match the residuals for the different terms in selected cases. In addition, the predictive power of the GMM is also analyzed by comparing the observed

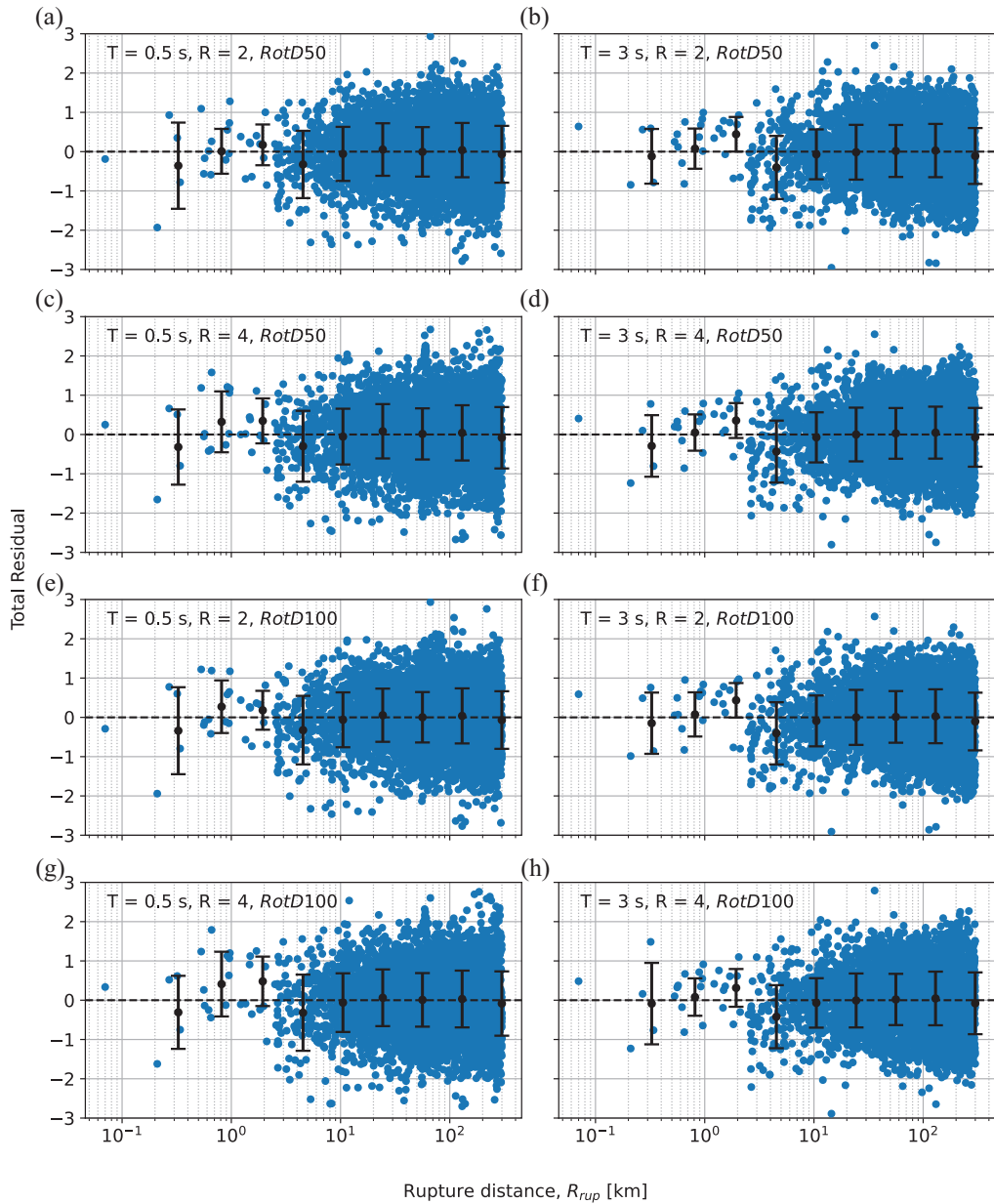


Figure 10. Total residuals with respect to R_{rup} for different T and R . Blue dots represent the observed residuals, while black dots and error bars represent the binned mean and \pm one standard deviation, respectively (color version available online).

and median predicted values of Sd_i for each system (i.e. different T and R). The results of this comparison are illustrated in Figure 12, where it can be seen that there is a very good match between the predicted and observed values. This is first clear from Figure 12 via how close the data points are to the bisector line with no significant bias. Also provided in Figure 12 is the coefficient of determination R^2 , which is observed to be around 0.8 for all the cases and no lower than 0.7.

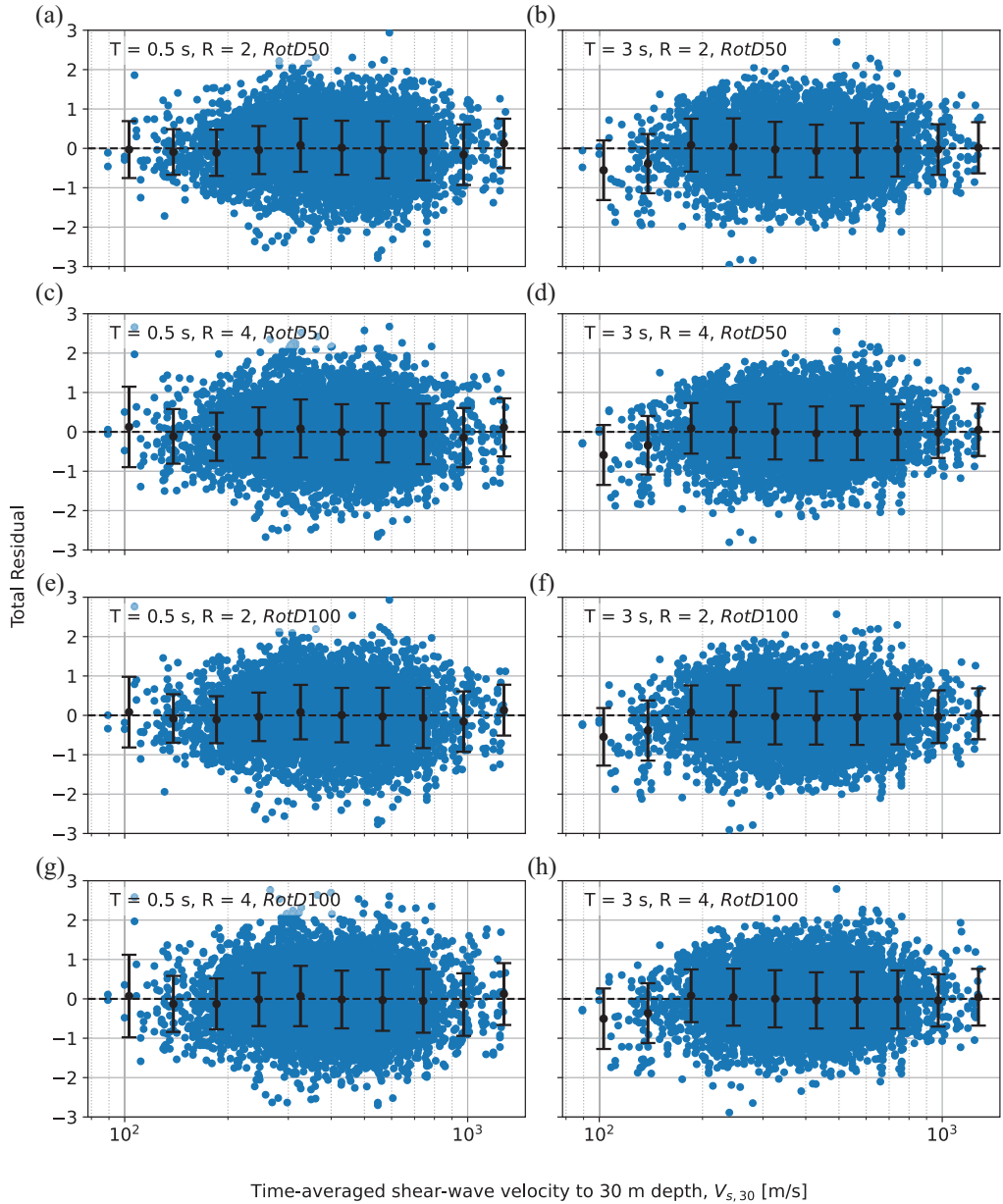


Figure 11. Total residuals with respect to $V_{s,30}$ for different T and R . Blue dots represent the observed residuals, while black dots and error bars represent the binned mean and \pm one standard deviation, respectively (color version available online).

Quantile–quantile (Q–Q) plots compare the quantile of each observation to the same quantity in the theoretical distribution. This is a well-established method to check if the data follow a certain theoretical distribution. If the data are linear and close to the diagonal identity line, then the chosen theoretical distribution is appropriate to describe the actual data. The Q–Q plot of the total logarithmic residuals for the case of $R = 4$ and $T = 1$ s is illustrated in Figure 13, where it can be seen that the natural logarithm of the

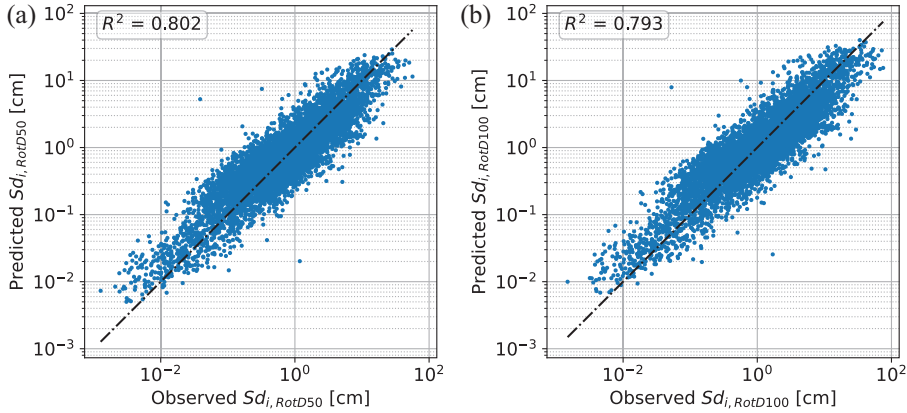


Figure 12. Observed (i.e. measured) versus predicted Sd_i in logarithmic axes. Case of $R = 4$ and $T = 1$ s. Blue dots represent the observed and predicted data points, while the black dash-dotted line represents the perfect fit.

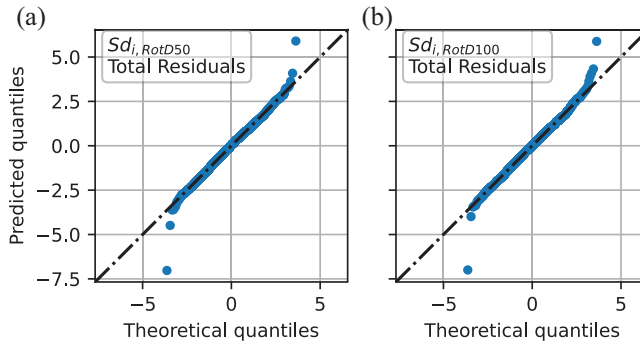


Figure 13. Q–Q plot of total residuals. Case of $R = 4$ and $T = 1$ s (color version available online).

predicted response values follows a normal distribution, confirming the suitability of the GMM developed.

Median inelastic spectra

With the proposed GMM, predictions for the median inelastic displacement spectra can be constructed, given specific GM causal parameters. Figure 14 shows the median inelastic displacement spectra for different R factors and four rupture scenarios. It can be seen that for short periods, inelastic displacements increase as R increases. This is observed up to a certain period, which changes depending on the scenario. For moderate- and long-period structures, the inelastic displacements are similar across the different R factors, essentially confirming the equal displacement approximation previously discussed. Needless to say, higher magnitudes and shorter distances produce higher spectral displacements, especially for increasing R values and increasing T . It can also be observed from Figure 14 that the median values of geometric mean are practically the same as the ones of the *RotD50* definition, with the geometric mean exhibiting slightly lower values in most of the period range.

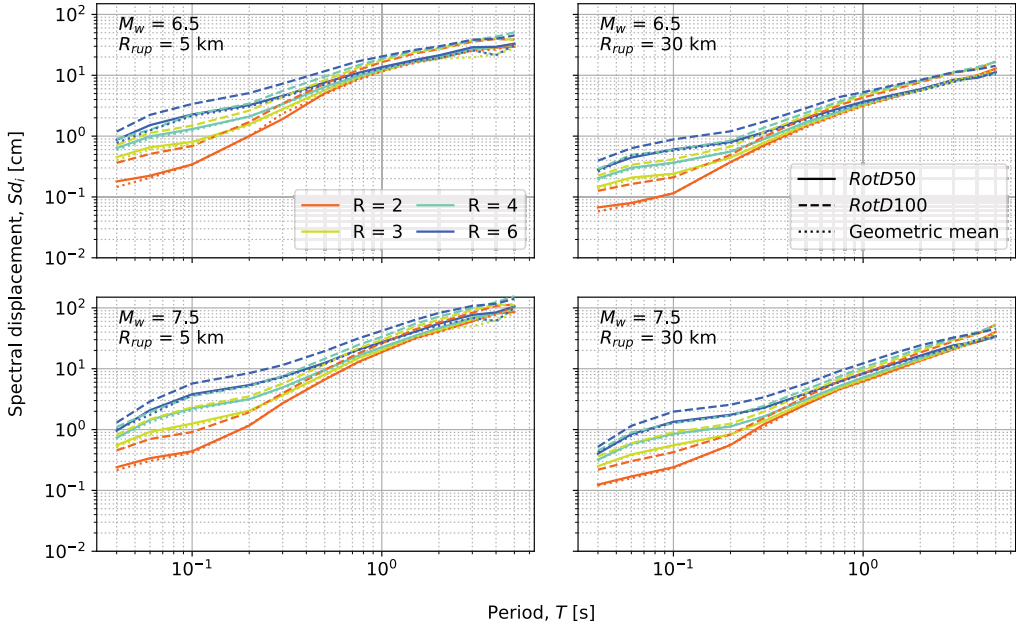


Figure 14. Median RotD50 and RotD100 inelastic displacement spectra for different scenarios (color version available online).

Comparison with previous studies

Using the developed GMM, some relative comparisons with existing models available in the literature were explored. Compared to other GMMs, this comparison presented some difficulties since it focused on inelastic spectral displacement. This IM does not have the same research on GMM development as other IMs such as spectral acceleration. Combining this also with the fact that the directionality aspect was incorporated presented some obstacles. Another difficulty was how none of the few available models quantified their inelastic displacement predictions in terms of the strength ratio R , instead using the ductility demand, μ , or the strength coefficient, C_y . Nonetheless, two models from the literature that predict inelastic spectral displacements were used for comparison with the model proposed herein. Namely, the models proposed by Tothong and Cornell (2006) and Huang et al. (2020), denoted as TC06 and HTG20.

First, starting with Tothong and Cornell (2006), this model uses the outputs of a conventional (elastic) GMM and then converts them to inelastic spectral displacements based on the proposed ratios. Hence, the model is actually just any conventional elastic spectral displacement GMM coupled with the TC06 inelastic displacement ratio model, with a proper statistical correlation between the two. Herein, the elastic GMM employed in the original article was used (Abrahamson and Silva, 1997), although in principle, any elastic GMM may be used. The predictive parameters are the rupture scenario parameters, the elastic period T , and a yield displacement, d_y . Regarding the bilinear oscillator, the main difference with this study is that 5% post-yield stiffness ratio was used. The maximum R_{rup} was limited to 95 km to avoid the potential effects of anelastic attenuation, as reported in the original article (Tothong and Cornell, 2006). The arbitrary horizontal component, $Sd_{i,arb}$, for each recording was selected.

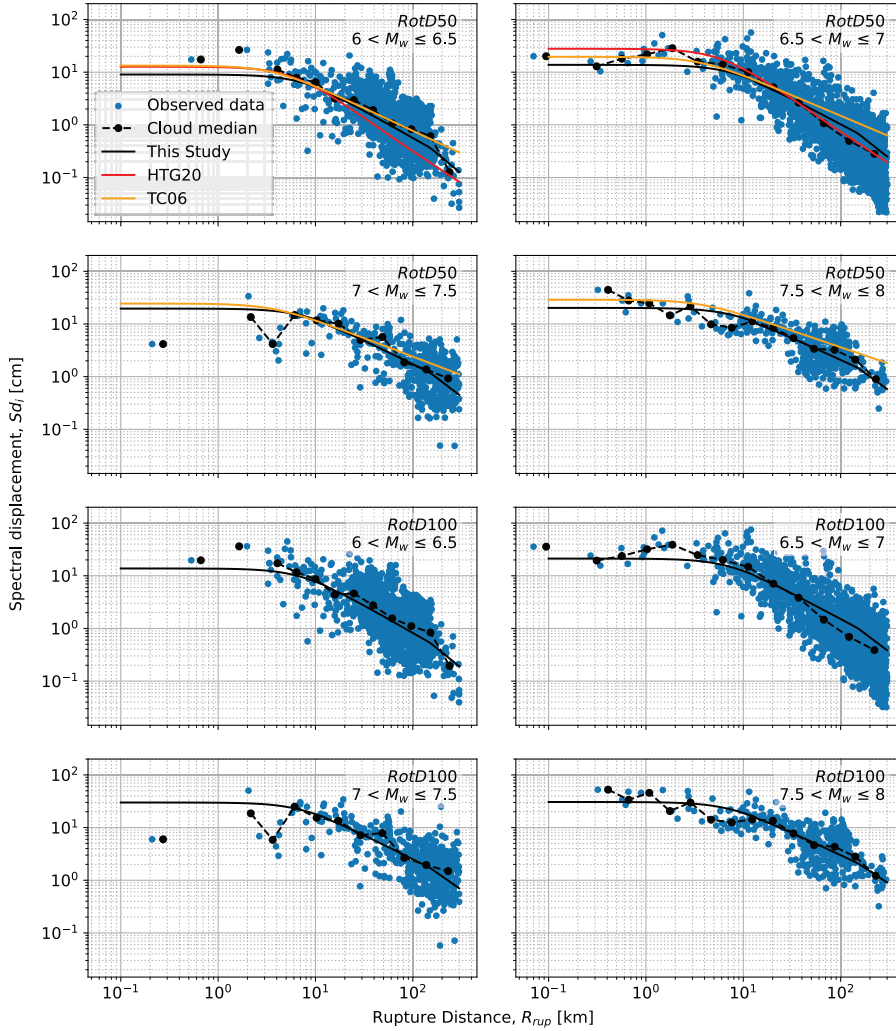


Figure 15. Median $S_{d_i, \text{RotD50}}$ predicted by the model, along with the empirical data, as a function of M_w and R_{rup} , for $T = 1$ s and $R = 4$ (color version available online).

In the study by Huang et al. (2020), they developed a region-specific GMM for northern Italy for inelastic spectral displacements, explicitly accounting for the spatial correlation between intra-event residuals. The strong motion database comprised of 2427 records from 85 events with magnitudes ranging from 4.0 to 6.4 and source-to-site distances less than 200 km. The geometric mean of the two horizontal components, $S_{d_{i, \text{gm}}}$, was used.

Four different comparisons are given in Figure 15 for the proposed GMM and the existing models from the literature. To better understand the quality of the fitting, GMs were divided into distinct magnitude bins and compared with the median predicted values corresponding to the mean magnitude of GMs contained in each bin. It can be observed that the median prediction of the proposed GMM generally matches well with the cloud median within the ranges containing a significant amount of data. The only exception is for $6.5 < M_w \leq 7$, where the model presents a little skewness from the cloud median. More amplified differences are observed at large distances since the model does not explicitly

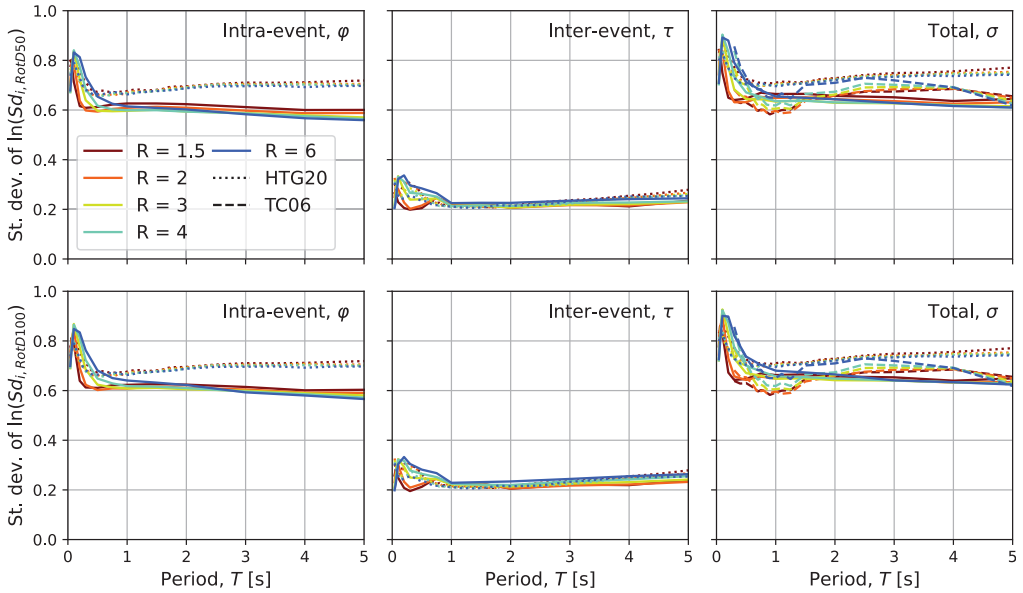


Figure 16. Intra-, inter-event, and total logarithmic standard deviations (color version available online).

account for anelastic attenuation effects and also at lower distances due to the scarcity of the data. The model of HTG20 is close to the proposed model for the two lower magnitude bins, but it was omitted from the comparisons for $M_w > 7$ because the earthquake magnitudes considered in the HTG20 model ranged from $4 < M_w \leq 6.4$. Meanwhile, the model of TC06 is quite close to the cloud median of the data, with the exception of overpredicting the displacements for moderate to long rupture distances. Again it is important to highlight that these models were predicting different GM components (i.e. $Sd_{i, \text{arb}}$ and $Sd_{i, \text{arb}}$) compared to the $Sd_{i, \text{RotD50}}$ being evaluated here.

GMM prediction uncertainty

An important part of any GMM is the variability around the median prediction, which were denoted in Equation 3 as τ to represent the inter-event term and ϕ to represent the intra-event standard deviations. This GMM uncertainty plays a crucial role in both the assessment of existing structures and design of new structures, as it can impact the median IM predictions with small mean annual rates of exceedance. Therefore, accurate quantification of the IM standard deviation is as important as the accurate estimation of its median value. Figure 16 shows the logarithmic standard deviations of the $\ln(Sd_{i, \text{RotD}_{nn}})$ estimations, where the intra- (ϕ), inter- (τ) and total (σ) logarithmic standard deviations are given, respectively. This representation adopts the homoscedasticity assumption commonly adopted (Boore et al., 2014; Campbell and Bozorgnia, 2014) in recent GMMs for Sa . It can be seen that the intra-event standard deviation is much higher than the inter-event one, naturally becoming the one principally driving the total standard deviation values. For $T < 1$ s, the total standard deviation increases as T decreases, whereas for $T > 1$ s there tended to be a plateau of about 0.65 ln (cm).

The total standard deviation values are compared with the corresponding ones of TC06. Since the standard deviation of that model depends on the magnitude, the mean

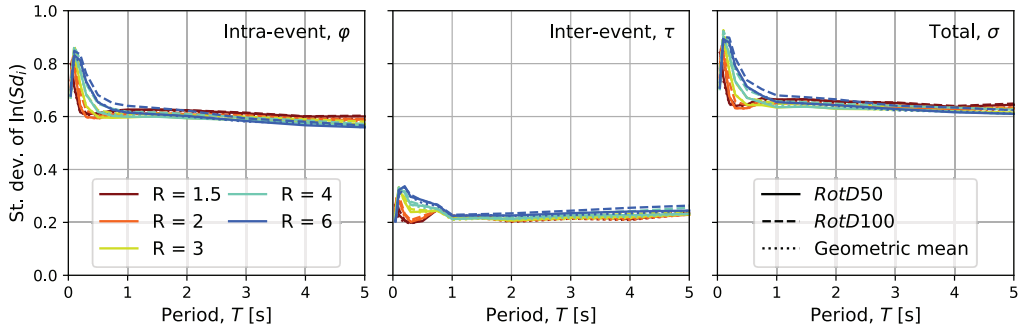


Figure 17. Effect of horizontal component definition on intra-, inter-event, and total logarithmic standard deviations (color version available online).

value of all the records considered in each case was utilized for relative comparison. It can be observed that for most values of T , the proposed model gives approximately the same order of magnitude of standard deviation as TC06, although slightly lower overall. The only exception is for $T \approx 1$ s, where the proposed model gives somewhat higher values. The lower values obtained here may be partially explained by the different definitions of horizontal component, as here the *RotD50* component was used, while in TC06 the arbitrary component of the recorded GM was used. This produces differences in standard deviation estimates as demonstrated in the study by Beyer and Bommer (2006) for elastic spectral ordinates, if the *GMRotD50* is assumed to have the same dispersion characteristics as *RotD50*. It was shown that the arbitrary component exhibits a higher standard deviation than the *GMRotD50*, especially for longer periods.

Regarding the comparison with HTG20, it can be seen that the HTG20 model's intra-event standard deviations are higher than the ones of the proposed model for $T > 0.5$ s, whereas the inter-event standard deviations have about the same values. The difference in total standard deviation is, therefore, primarily due to the difference in the intra-event standard deviation. Overall, the slightly smaller dispersion for most periods is a notable benefit of this GMM.

It should be noted that, according to Beyer and Bommer (2006), for elastic spectral values, the *GMRotD50* component exhibits only very slightly lower dispersion than the geometric mean of arbitrarily oriented components, while the median values are shown to be close, and conventionally equal for practical purposes. However, Figure 17 shows that for Sd_i the geometric mean exhibits about the same total standard deviation with the *RotD50*, if not even slightly lower at a few periods. Also illustrated in Figure 17 is the comparison with the *RotD100* component, which generally exhibits somewhat higher σ when compared to the *RotD50* component, especially in the middle and low periods.

Summary and conclusion

This article has looked at the inelastic spectral displacement demands caused by shallow crustal earthquakes considering GM directionality effects. The first part of the article examined the general directionality trends of GMs in the NGA-West2 database for a range of inelastic SDOF systems. The inelastic displacement spectra were computed for the *RotD100*, *RotD50*, and *RotD00* definitions of horizontal GM and plotted against the

corresponding elastic ones. These spectra provided important insights into the response directionality of such systems and their relationship with the elastic ones. A comparison of traditional nonlinear response models with the results obtained herein, which consider the directionality effects, was also demonstrated. The second part of this article presented a new GMM using the previous results to predict the *RotD50* and *RotD00* definitions of horizontal GM for SDOF inelastic spectral displacements, namely $Sd_{i, \text{RotD50}}$ and $Sd_{i, \text{RotD100}}$, as a function of the initial elastic period of vibration, T , strength ratio, R , and a set of source, path, and site effect parameters. This model was evaluated and compared with other relatively similar models available in the literature. The proposed GMM can be utilized in scenario and probabilistic seismic hazard analyses to generate inelastic displacement spectra directly. Based on these developments, the following can be noted:

- The effect of directionality, quantified via the *RotD100*/*RotD50* ratio, on elastic systems was observed to be the same as the results obtained previously by Shahi and Baker (2014). For the inelastic systems, this ratio increased with R for $T > 0.3$ s, whereas the opposite and more pronounced trend was observed for $T < 0.3$ s.
- Examining a subset of near-fault GMs showed higher elastic and inelastic displacements $Sd_{i, \text{RotDmn}}$ and higher directionality for the entire range of T , which is a somewhat expected result.
- Comparing these inelastic SDOF system demands in terms of strength ratio, ductility, and period meant that they could be compared with traditional R - μ - T relationships found in several past studies, methods, and codes of practice. Overall, it was seen that studies tended to underestimate the nonlinear demands in the SDOF system by virtue of the component definition (either arbitrary or geometric mean) that they utilized.
- For what concerns the GMM developed to represent the *RotD50* and *RotD100* components of inelastic spectral displacement demand, a mixed-effects regression model was fitted to capture the behavior with very good accuracy.
- The proposed GMM exhibited reasonably low dispersions when compared with others available in the literature and is not sensitive to the level of nonlinear demand. Compared to past models, this GMM was fitted using a substantially large set of GMs from the NGA-West2 database. It also does not require any auxiliary elastic GMM to predict the median and dispersion of inelastic displacements.
- The range of applicability of this GMM is the following: moment magnitude, $5 < M_w \leq 8$; rupture distance, $0 < R_{\text{rup}} \leq 300$ km; average shear-wave velocity in the top 30 m of the site profile, $90 \leq V_{s,30} \leq 1300$ m/s; tectonically active shallow crustal regions; period of vibration, $0.04 \leq T \leq 5$ s; and strength ratio, $1 < R \leq 6$.

The proposed GMM can be utilized in both deterministic and probabilistic seismic hazard analyses to directly generate inelastic displacement spectra. However, it should be noted that for a regional portfolio assessment it may be challenging to reliably estimate the strength ratio of each building typology, but as it is argued that an approximate yet representative value for a particular building portfolio class would still suffice for practical purposes. Nonetheless, for a single building, whose global behavior can be easily broken down to a bilinear SDOF system with a specific period and strength ratio, the IMs proposed herein can be very effective in predicting the structural response.

Acknowledgments

The authors would like to acknowledge the two anonymous reviewers for their valuable comments and suggestions that have contributed to increase the value of this article.

Author's note

The work presented in this article has been developed within the framework of the project “Dipartimenti di Eccellenza.”


Declaration of conflicting interests


The author(s) declared no potential conflicts of interest with respect to the research, authorship, and/or publication of this article.

Funding

The author(s) disclosed receipt of the following financial support for the research, authorship, and/or publication of this article: this work has been funded by the Italian Ministry of Education, University and Research at IUSS Pavia.

ORCID iDs

Savvinos Aristeidou  <https://orcid.org/0000-0002-4224-7891>

Gerard J O'Reilly  <https://orcid.org/0000-0001-5497-030X>

Data availability statement/Electronic supplement

Electronic supplement for the GMM functional form coefficients: “GMM_coefficients.xlsx.”
Electronic supplement for the inelastic directionality model median and standard deviations: “inel_dirac_model.xlsx.”

References

- Abrahamson NA and Silva WJ (1997) Empirical response spectral attenuation relations for shallow crustal earthquakes. *Seismological Research Letters* 68(1): 94–127.
- Abrahamson NA and Silva WJ (2008) Summary of the Abrahamson & Silva NGA ground-motion relations. *Earthquake Spectra* 24(1): 67–97.
- Abrahamson NA and Youngs RR (1992) A stable algorithm for regression analyses using the random effects model. *Bulletin of the Seismological Society of America* 82(1): 505–510.
- Ahdi SK, Mazzoni S, Kishida T, Wang P, Nweke CC, Kuehn NM, Contreras V, Rowshandel B, Stewart JP and Bozorgnia Y (2020) Engineering characteristics of ground motions recorded in the 2019 Ridgecrest earthquake sequence. *Bulletin of the Seismological Society of America* 110(4): 1474–1494.
- American Society of Civil Engineers (ASCE)/SEI 7-16 (2018) Minimum design loads for buildings and other structures.
- Ancheta TD, Darragh RB, Stewart JP, Seyhan E, Silva WJ, Chiou BSJ, Wooddell KE, Graves RW, Kottke AR, Boore DM, Kishida T and Donahue JL (2013) *PEER NGA-West2 database*. Technical report PEER 2013/03, 2 May. Berkeley, CA: Pacific Earthquake Engineering Research (PEER) Center, University of California, Berkeley.
- Aslani H and Miranda E (2005) *Probabilistic Earthquake Loss Estimation and Loss Disaggregation in Buildings*. Stanford, CA: Department of Civil and Environmental Engineering, Stanford University.

- Baker JW and Cornell CA (2005) A vector-valued ground motion intensity measure consisting of spectral acceleration and epsilon. *Earthquake Engineering & Structural Dynamics* 34(10): 1193–1217.
- Baker JW and Cornell CA (2006) Which spectral acceleration are you using? *Earthquake Spectra* 22(2): 293–312.
- Baker JW and Lee C (2018) An improved algorithm for selecting ground motions to match a conditional spectrum. *Journal of Earthquake Engineering* 22(4): 708–723.
- Beyer K and Bommer JJ (2006) Relationships between median values and between aleatory variabilities for different definitions of the horizontal component of motion. *Bulletin of the Seismological Society of America* 96(4A): 1512–1522.
- Boore DM (2010) Orientation-independent, nongeometric-mean measures of seismic intensity from two horizontal components of motion. *Bulletin of the Seismological Society of America* 100(4): 1830–1835.
- Boore DM, Stewart JP, Seyhan E and Atkinson GM (2014) NGA-West2 equations for predicting PGA, PGV, and 5% damped PSA for shallow crustal earthquakes. *Earthquake Spectra* 30(3): 1057–1085.
- Boore DM, Watson-Lamprey J and Abrahamson NA (2006) Orientation-independent measures of ground motion. *Bulletin of the Seismological Society of America* 96(4A): 1502–1511.
- Bozorgnia Y, Abrahamson NA, Al Atik L, Ancheta TD, Atkinson GM, Baker JW, Baltay AS, Boore DM, Campbell KW, Chiou BSJ, Darragh RB, Day S, Donahue J, Graves RW, Gregor N, Hanks TC, Idriss IM, Kamai R, Kishida T, Kottke A, Mahin SA, Rezaeian S, Rowshandel B, Seyhan E, Shahi SK, Shantz T, Silva W, Spudich PA, Stewart JP, Watson-Lamprey J, Wooddell K and Youngs R (2014) NGA-West2 research project. *Earthquake Spectra* 30(3): 973–987.
- Bozorgnia Y, Hachem MM and Campbell KW (2010) Ground motion prediction equation (“Attenuation Relationship”) for inelastic response spectra. *Earthquake Spectra* 26(1): 1–23.
- Bradley BA (2010) A generalized conditional intensity measure approach and holistic ground-motion selection. *Earthquake Engineering & Structural Dynamics* 39(12): 1321–1342.
- Bradley BA (2012) The seismic demand hazard and importance of the conditioning intensity measure. *Earthquake Engineering & Structural Dynamics* 41(11): 1417–1437.
- Bradley BA and Baker JW (2014) Ground motion directionality in the 2010–2011 Canterbury earthquakes. *Earthquake Engineering & Structural Dynamics* 44(3): 371–384.
- Bray JD and Rodriguez-Marek A (2004) Characterization of forward-directivity ground motions in the near-fault region. *Soil Dynamics and Earthquake Engineering* 24(11): 815–828.
- Burks LS and Baker JW (2014) Validation of ground-motion simulations through simple proxies for the response of engineered systems. *Bulletin of the Seismological Society of America* 104(4): 1930–1946.
- Campbell KW and Bozorgnia Y (2007) *Campbell-Bozorgnia NGA Ground Motion Relations for the Geometric Mean Horizontal Component of Peak and Spectral Ground Motion Parameters*. Berkeley, CA: Pacific Earthquake Engineering Research Center (PEER), University of California, Berkeley.
- Campbell KW and Bozorgnia Y (2014) Campbell-Bozorgnia NGA-West2 horizontal ground motion model for active tectonic domains. In: *Proceedings of the 10th US national conference on earthquake engineering: Frontiers of earthquake engineering (NCEE 2014)*, Anchorage, AK, 21–25 July.
- Chopra AK (2014) *Dynamics of Structures—Theory and Applications to Earthquake Engineering*. 4th ed. Harlow: Pearson Education Limited.
- Fontara I-KM, Kostinakis KG, Manoukas GE and Athanatopoulou AM (2015) Parameters affecting the seismic response of buildings under bi-directional excitation. *Structural Engineering and Mechanics* 53(5): 957–979.
- Heresi P, Dávalos H and Miranda E (2018) Ground motion prediction model for the peak inelastic displacement of single-degree-of-freedom bilinear systems. *Earthquake Spectra* 34(3): 1177–1199.
- Huang C, Tarbali K and Galasso C (2020) A region-specific ground-motion model for inelastic spectral displacement in northern Italy considering spatial correlation properties. *Seismological Research Letters* 92(3): 1979–1991.

- Huang YN, Whittaker AS and Luco N (2009) Orientation of maximum spectral demand in the near-fault region. *Earthquake Spectra* 25(3): 707–717.
- Kaklamanos J, Baise LG and Boore DM (2011) Estimating unknown input parameters when implementing the NGA ground-motion prediction equations in engineering practice. *Earthquake Spectra* 27(4): 1219–1235.
- Luco N and Cornell CA (2007) Structure-specific scalar intensity measures for near-source and ordinary earthquake ground motions. *Earthquake Spectra* 23(2): 357–392.
- Miranda E and Bertero VV (1994) Evaluation of strength reduction factors for earthquake-resistant design. *Earthquake Spectra* 10: 357–379.
- Nafeh AMB, O'Reilly GJ and Monteiro R (2020) Simplified seismic assessment of infilled RC frame structures. *Bulletin of Earthquake Engineering* 18: 1579–1611.
- Nassar AA and Krawinkler H (1991) *Seismic demands for SDOF and MDOF systems*. Report no. 95, June, p. 204. Stanford, CA: Stanford University.
- Newmark NM and Hall WJ (1982) *Earthquake Spectra and Design*. Berkeley, CA: Earthquake Engineering Research Institute (EERI).
- O'Reilly GJ (2021) Seismic intensity measures for risk assessment of bridges. *Bulletin of Earthquake Engineering* 19(9): 3671–3699.
- Rupakhety R and Sigbjörnsson R (2009) Ground-motion prediction equations (GMPEs) for inelastic response and structural behaviour factors. *Bulletin of Earthquake Engineering* 7(3): 637–659.
- Rupakhety R and Sigbjörnsson R (2013) Rotation-invariant measures of earthquake response spectra. *Bulletin of Earthquake Engineering* 11(6): 1885–1893.
- Shahi SK and Baker JW (2014) NGA-West2 models for ground motion directionality. *Earthquake Spectra* 30(3): 1285–1300.
- Stafford PJ, Sullivan TJ and Pennucci D (2016) Empirical correlation between inelastic and elastic spectral displacement demands. *Earthquake Spectra* 32(3): 1419–1448.
- Tarbali K (2017) *Ground motion selection for seismic response analysis*. PhD Thesis, University of Canterbury, Christchurch, New Zealand.
- Tarbali K, Bradley BA and Baker JW (2019) Ground motion selection in the near-fault region considering directivity-induced pulse effects. *Earthquake Spectra* 35(2): 759–786.
- Tothong P and Cornell CA (2006) An empirical ground-motion attenuation relation for inelastic spectral displacement. *Bulletin of the Seismological Society of America* 96(6): 2146–2164.
- Vamvatsikos D and Cornell CA (2005) Developing efficient scalar and vector intensity measures for IDA capacity estimation by incorporating elastic spectral shape information. *Earthquake Engineering & Structural Dynamics* 34(13): 1573–1600.
- Vamvatsikos D and Cornell CA (2006) Direct estimation of the seismic demand and capacity of oscillators with multi-linear static pushovers through IDA. *Earthquake Engineering & Structural Dynamics* 35(9): 1097–1117.
- Vidic T, Fajfar P and Fischinger M (1994) Consistent inelastic design spectra: Strength and displacement. *Earthquake Engineering & Structural Dynamics* 23(5): 507–521.
- Zengin E and Abrahamson NA (2021) A procedure for matching the near-fault ground motions based on spectral accelerations and instantaneous power. *Earthquake Spectra* 37(4): 2545–2561.
- Zhu M, McKenna F and Scott MH (2018) OpenSeesPy: Python library for the OpenSees finite element framework. *SoftwareX* 7: 6–11.